scientific reports

Check for updates

OPEN

Numerical study of bio-convection flow of magneto-cross nanofluid containing gyrotactic microorganisms with activation energy

Qiu-Hong Shi[1], Aamir Hamid[2], M. Ijaz Khan[3], R. Naveen Kumar[4], R. J. Punith Gowda[4], B. C. Prasannakumara[4], Nehad Ali Shah[5,6]✉, Sami Ullah Khan[7] & Jae Dong Chung[5]

In this study, a mathematical model is developed to scrutinize the transient magnetic flow of Cross nanoliquid past a stretching sheet with thermal radiation effects. Binary chemical reactions and heat source/sink effects along with convective boundary condition are also taken into the consideration. Appropriate similarity transformations are utilized to transform partial differential equations (PDE's) into ordinary ones and then numerically tackled by shooting method. The impacts of different emerging parameters on the thermal, concentration, velocity, and micro-rotation profiles are incorporated and discussed in detail by means of graphs. Results reveal that, the escalation in magnetic parameter and Rayleigh number slowdowns the velocity and momentum of the fluid. The increase in Biot number, radiation and heat sink/source parameters upsurges the thermal boundary but, converse trend is seen for escalating Prandtl number. The density number of motile microorganisms acts as a growing function of bioconvection Lewis number and declining function of bioconvection Peclet number.

Researchers and scientists nowadays have more research fields due to developments in nanotechnology and nanoscience. Nanofluids are proving to be useful in a variety of situations, including heat transference, technological advances demand efficient heat conveyance processes, and nanoliquids provide a more effective medium for heat passage from one source to the other. In this regard different fluid models have been presented over time to illustrate fluid properties. The Cross-viscosity model for generalized Newtonian fluid was proposed by Cross. By using this concept, Khan et al.[1] elucidated the chemically reacting magnetohydrodynamic (MHD) radiative flow of cross nanoliquid towards a stretchy sheet. Ali et al.[2] explicated the radiative stream of cross nanoliquid instigated by a stretchy sheet. Abbas et al.[3] expounded the MHD convective stream of cross nanoliquid with thermal radiation. Xiong et al.[4] illuminated the chemically reacting dissipative flow of cross nanoliquid with mixed convection. Hamid et al.[5] investigated the axisymmetric stream of cross nanoliquid flow with radiation and chemical reaction effect.

The studies of magnetohydrodynamic (MHD) streams of non-Newtonian and Newtonian liquids over a stretching surface have gotten a lot of interest because of their wide range of uses in chemical engineering and metallurgy. Such MHD flow investigations are critical in industry and have uses in a number of fields, including petroleum processing and metallurgical processes. The rate of cooling, as well as the desired end product properties, can be regulated by using electrically conducting fluids and applying a magnetic field. In the purification of molten metals from nonmetallic inclusions, a magnetic field has been used. Recently, Hayat et al.[6] elucidated the MHD radiative stream of liquid past a porous stretchy sheet with thermal radiation. Senapati et al.[7] expounded

[1]Department of Mathematics, Huzhou University, Huzhou 313000, People's Republic of China. [2]Department of Mathematics, Quaid-i-Azam University, Islamabad 44000, Pakistan. [3]Department of Mathematics and Statistics, Riphah International University, I-14, Islamabad 44000, Pakistan. [4]Department of Studies and Research in Mathematics, Davangere University, Davangere, Karnataka, India. [5]Department of Mechanical Engineering, Sejong University, Seoul 05006, Korea. [6]Department of Mathematics, Lahore Leads University, Lahore, Pakistan. [7]Department of Mathematics, COMSATS University Islamabad, Sahiwal 57000, Pakistan. ✉email: nehadali199@yahoo.com

the MHD flow of Casson nanoliquid flow above a stretch sheet. Patil et al.[8] deliberated the chemically reacting radiative stream of Powel–Eyring liquid above a stretchy sheet. Uddinet al.[9] elucidated the MHD radiative stream of Prandtl–Eyring nanoliquid above a stretchy sheet with mixed convection. Nayak et al.[10] explicated the MHD steam of micropolar Casson cross nanoliquid.

The mechanism of thermal radiation involves a hot body releasing electromagnetic radiation in both directions. Many objects on the planet emit radiation in the infrared range of the electromagnetic spectrum. Thermal radiation is important in heat nuclear reactor protection, power plants, exchangers, furnace architecture, solar energy, and power technology. Motivated by these uses, Khan et al.[11] explored the radiative flow of Carreau liquid above a stretchy surface. Hashim et al.[12] explicated the radiative stream of Williamson nanoliquid above a stretchy geometry. Ali et al.[13] elucidated the radiative flow of nanoliquid with heat production/absorption. Reddy et al.[14] expounded the radiative flow of nanoliquid past a melting surface. Xionget al.[15] explicated the effect of radiation and heat source/sink on flow of hybrid nanoliquid.

The relationships between chemical reactions and mass transport are typically complex, as shown by the synthesis and absorption of reactant species at various rates both within the liquid and during mass transfer. Chemical reactions have abundant usages in fields of engineering and sciences like electric power generator and food processing. The concept of binary chemical reaction was initially elucidated by Merkin[16]. Rasool et al.[17] exemplified the impact of binary chemical reaction on Williamson nanoliquid above anelastic sheet. Wang et al.[18] elucidated the chemically reactive dissipative stream of Carreau nanoliquid above a stretchy surface. Gowda et al.[19] expounded the impact of chemical reaction on nanoliquid stream past a stretchy sheet coiled in a circle. Khan and Alzahrani[20] expounded the impact of binary chemical reaction on radiative stream of Walter-B nanoliquid.

Bio-convection is a natural process that occurs as microorganisms move randomly in single-celled or colony-like formation. The directional motion of various forms of microorganisms is the basis for various bio-convection systems. Gyrotactic microorganisms are those that swim upstream against gravity in still water, causing the upper portion of the suspension to be denser than the lower part. Bioconvection's importance can be seen in a variety of bio-microsystems, such as biotechnology related to mass transportation, enzyme biosensors and mixing. Recently, Khan et al.[21] elucidated the MHD bioconvective stream of Newtonian fluid with chemical reaction. Chu et al.[22] explicated the MHD bioconvective stream of third grade liquid past a stretchy sheet by using Buongiorno model. Al-Khaled et al.[23] expounded the radiative bioconvective stream of nanoliquid. Zadeh et al.[24] elucidated the bioconvectionflow of micropolar liquid instigated by anupright sheet. Waqas et al.[25] explicated bioconvective stream of second-grade nanofluid with radiation effect.

It is familiar that there are various approaches that could be contemplated in order to explain few realistic solutions for this specific type of issue. However, to the best of the authors' understanding, no numerical solution has been earlier inspected for magnetic flow of Cross nanofluid past a stretching sheet with thermal radiation effects. Also, the findings of this research are completely new and have never been published previously. The focal point in the current paper is to examine the above-described flow numerically. Our findings from this research are likely to provide not only useful information for applications, but also a supplement to the current literature. These impacts will be unique and novel, according to the most effective of our data.

Mathematical formulation

In this study, we have considered transient two-dimensional magnetic flow of an incompressible Cross nanofluid past a stretching sheet in the presence of thermal radiation effects. A non-uniform time dependent transverse magnetic field of strength B_0 is applied perpendicular to flow direction (see Fig. 1 [26]). Since the magnetic Reynolds number is low, the induced magnetic field can be ignored. The effect of Brownian motion and thermophoresis is incorporated into a currently developed framework for nanofluid. The implementation of a critical practical concentration condition, namely the zero nanoparticles mass flux condition and also, the convective boundary condition are taken into consideration. Binary chemical reactions and heat source/sink effects are also taken into consideration. The suspension of nanoparticles in nanofluid is achieved through the use of a surfactant or surface charge technology. This prevents nanoparticles from adhering to the surface and accumulating.

The governing equations of the above-described flow are[1–4]:

Continuity:

$$\frac{\partial u}{\partial x}+\frac{\partial u}{\partial y}=0. \tag{1}$$

Momentum equation:

$$\frac{\partial u}{\partial t}+u\frac{\partial u}{\partial x}+v\frac{\partial u}{\partial y}=\nu\left[\frac{\frac{\partial u}{\partial y}}{1+\left\{\Gamma\left(\frac{\partial u}{\partial y}\right)^{1-n}\right\}^{2}}\right]-\frac{\sigma B^{2}(t)}{\rho_f}u+\frac{1}{\rho_f}\begin{bmatrix} g\rho_f(T-T_\infty)\beta(1-C_\infty) \\ -g(\rho_p-\rho_f)(C-C_\infty) \\ -g(\rho_m-\rho_\infty)\gamma(n-n_\infty)\end{bmatrix}. \tag{2}$$

Energy equation:

$$\frac{\partial T}{\partial t}+u\frac{\partial T}{\partial x}+v\frac{\partial T}{\partial y}=\left[\alpha_f+\frac{16\sigma^{*}T_\infty^{3}}{3k^{*}\left(\rho c_f\right)}\frac{\partial^{2}T}{\partial y^{2}}\right]+\tau\left[D_B\frac{\partial C}{\partial r}\frac{\partial T}{\partial r}+\frac{D_T}{T_\infty}\left(\frac{\partial T}{\partial r}\right)^{2}\right]+\frac{Q_0}{\left(\rho c_p\right)_f}\left[(T-T_\infty)\right]. \tag{3}$$

Concentration equation:

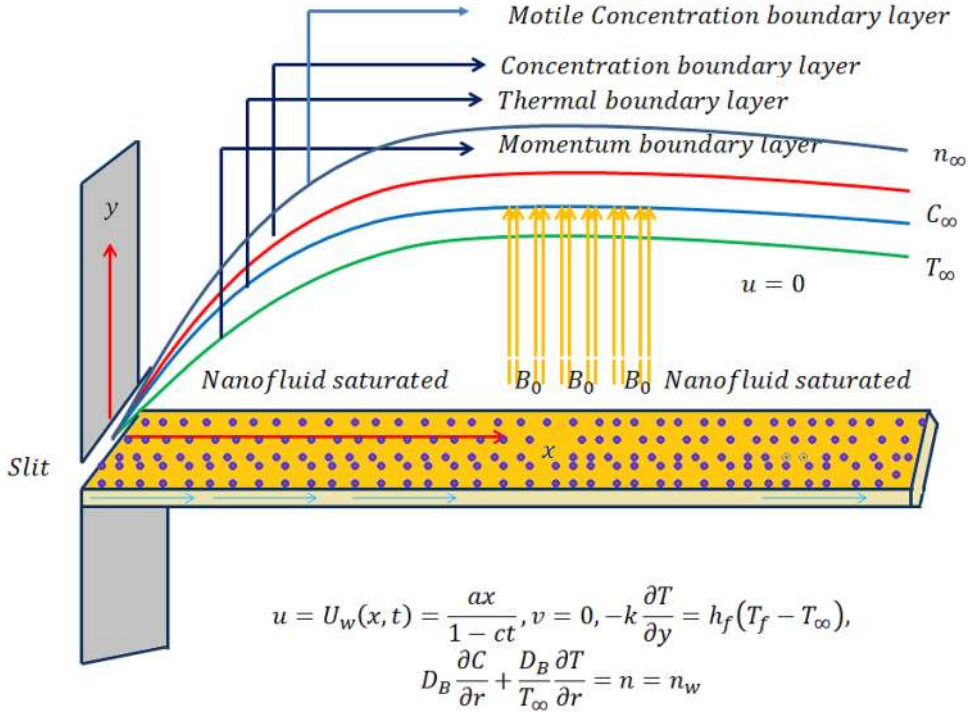

Figure 1. Schematic sketch of the physical model.

$$\frac{\partial C}{\partial t} + u\frac{\partial C}{\partial x} + v\frac{\partial C}{\partial y} = D_B\frac{\partial^2 C}{\partial y^2} + \frac{D_T}{T_\infty}\left(\frac{\partial^2 C}{\partial y^2}\right) - k_r^2(C - C_\infty)\left(\frac{T}{T_\infty}\right)^{n^*}\exp\left(-\frac{E_a}{k^*T}\right). \tag{4}$$

Bioconvection equation:

$$\frac{\partial n}{\partial t} + u\frac{\partial n}{\partial x} + v\frac{\partial n}{\partial y} + \frac{b_1 W_c}{C_\infty}\left[\frac{\partial}{\partial y}\left(n\frac{\partial C}{\partial r}\right)\right] = D_m\left(\frac{\partial^2 n}{\partial y^2}\right). \tag{5}$$

The physical realistic boundary conditions are

$$u = U_w(x,\, t) = \frac{ax}{1-ct},\ v = 0,\ -k\frac{\partial T}{\partial y} = h_f\left(T_f - T_\infty\right),\ D_B\frac{\partial C}{\partial r} + \frac{D_T}{T_\infty}\frac{\partial T}{\partial r} = 0,\ n = n_w \text{ at } y = 0, \tag{6}$$

$$u \to 0,\ T \to T_\infty,\ C \to C_\infty,\ n \to n_\infty \text{ as } y \to \infty. \tag{7}$$

We have the similarity transformations

$$\eta = y\sqrt{\frac{U_w}{\nu x}},\ \psi = \sqrt{\nu U_w x} f(\eta),\ \theta(\eta) = \frac{T - T_\infty}{T_f - T_\infty},\ \phi(\eta) = \frac{C - C_\infty}{C_\infty},\ \chi(\eta) = \frac{n - n_\infty}{n_w - n_\infty}. \tag{8}$$

The stream function $\psi(r,\, x)$ is given by $u = \frac{1}{r}\frac{\partial \psi}{\partial r}$ and $v = -\frac{1}{r}\frac{\partial \psi}{\partial x}$,

By utilizing Eq. (8) in Eqs. (1)–(5) with associated boundary constraints revealed in Eqs. (6) and (7), we came to know that Eq. (1) is satisfied and Eqs. (2–5) take the following form

$$\begin{aligned}&(ff'' - (f')^2)[1 + (Wef'')^{1-n}] - M^2 f'\left[1 + (Wef'')^{1-n}\right] + [1 + n(Wef'')^{1-n}]f''' \\ &- A\left(f' + \frac{\eta}{2}f''\right) + \lambda(\theta - N_r\phi - R_b\chi) = 0,\end{aligned} \tag{9}$$

$$\left(1 + \frac{4}{3}Rd\right)\frac{1}{\Pr}\theta'' + f\theta' + A\frac{\eta}{2}\theta' + N_b\theta'\phi' + N_t\theta'^2 + Q_0\theta = 0, \tag{10}$$

$$\phi'' + Scf\phi' + \frac{N_t}{N_b}\theta'' + ScA\frac{\eta}{2}\phi' - \sigma(1 + \delta\theta)^{n^*}\phi\exp\left(-\frac{E_1}{1 + \delta\theta}\right) = 0, \tag{11}$$

$$\chi'' + Lbf\chi' - Pe\left[\chi'\phi' + (\chi + \Omega)\right] + LbA\frac{\eta}{2}\chi' = 0, \tag{12}$$

and transformed boundary conditions are:

$$f(0) = 0,\ f'(0) = 1,\ \theta'(\eta) = -Bi[1 + \theta(\eta)],\ N_b\phi' + N_t\theta' = 0, \chi(0) = 1, \tag{13}$$

$$f'(\infty) \to 0,\ \theta(\infty) \to 0,\ \phi(\infty) \to 0,\ \chi(\infty) \to 0, \tag{14}$$

where, prime denotes the derivative with respect to η and the dimensionless physical parameters are defined as follows:

$M = \frac{\sigma B_0^2}{2\rho a}$ is the magnetic parameter, $Lb = \left(\frac{\alpha}{D_n}\right)$ is bioconvection Lewis number, $Rd = \frac{4\sigma^* T_\infty^3}{3k^* k_f}$ denotes the radiation parameter, $We = a\Gamma Re^{1/2}$ is the Weissenberg number, $Q_0 = \left(\frac{Q(1-ct)}{a(\rho c)_f}\right)$ heat generation/absorption parameter, $Nb = \left(\frac{\tau D_B(C_f - C_\infty)}{\nu}\right)$ Brownian motion parameter, $A = \left(\frac{c}{a}\right)$, unsteadiness parameter, $Sc = \left(\frac{\nu}{D_B}\right)$ the Schmidt number, $\Pr = \left(\frac{\mu c_p}{k}\right)$, Prandtl number, $Pe = \left(\frac{b_1 W_c}{D_n}\right)$ the bioconvection Peclet number, $Le = \left(\frac{\alpha}{D_B}\right)$ the traditional Lewis number, $Nt = \left(\frac{\tau D_B(T_f - T_\infty)}{\nu T_\infty}\right)$ the thermophoresis parameter, $N_r = \left(\frac{(\rho_p - \rho_f)\Delta C_w}{\rho_f \beta(1-C_\infty)\Delta T_f}\right)$ the buoyancy ratio parameter, $Rb = \left(\frac{\gamma\Delta\rho\Delta n_w}{\rho_f\beta(1-C_\infty)\Delta T_f}\right)$ the bioconvection Rayleigh number, $\sigma = \left(\frac{n_\infty}{\Delta n_w}\right)$ the bioconvection constant.

It should be remembered that the physical quantities of engineering concern, namely the local skin friction coefficient, local Nusselt quantity, and motile microorganisms, are also essential characteristics of the current investigation.

$$C_f = \frac{\tau_w}{\rho U_w^2},\ Nu_x = \frac{xq_w}{k_f\left(T_f - T_\infty\right)},\ Nn_x = \frac{xq_n}{D_n(n_w - n_\infty)}, \tag{15}$$

where τ_w, q_w, q_n is the wall shear stress and wall heat flux and wall motile microorganism flux, respectively, having the following form:

$$\tau_w = \mu_0\left(\frac{\frac{\partial u}{\partial y}}{1 + \left\{\Gamma\left(\frac{\partial u}{\partial y}\right)^{1-n}\right\}}\right)_{y=0},\ q_w = -k\left(\frac{\partial T}{\partial y}\right)_{y=0},\ q_n = -D_n\left(\frac{\partial n}{\partial y}\right)_{y=0}. \tag{16}$$

Following relations in dimensionless form are:

$$Re^{1/2}C_f = \frac{2f''(0)}{[1 + \left\{Wef''(0)\right\}^{1-n}]},\ Re^{-1/2}Nu_x = -\left(1 + \frac{4}{3}Rd\right)\theta'(0),\ Re^{-1/2}Nn_x = -\chi'(0). \tag{17}$$

Numerical scheme

The numerical simulations are presented in this section by using shooting technique. On this end, the formulated problem is converted into first order differential equations by making following assumptions:

$$\left.\begin{aligned} &f = z_1, f' = z_2, f'' = z_3, f''' = z_3^{'},\\ &\theta = z_4,\ \theta' = z_5, \theta'' = z_5^{'},\\ &\phi = z_6,\ \phi' = z_7, \phi'' = z_7^{'},\\ &\chi = z_8,\ \chi' = z_9, \chi'' = z_9^{'}. \end{aligned}\right\} \tag{18}$$

In view of above assumptions, Eqs. (10–14) yield:

$$z_3^{'} = \frac{-\left(z_1z_3 - (z_2)^2\right)[1 + (Wez_3)^{1-n}] + M^2z_2\left[1 + (Wez_3)^{1-n}\right] + A\left(z_2 + \frac{\eta}{2}z_3\right) - \lambda(z_4 - N_rz_6 - R_bz_8)}{\left(1 + n(Wez_3)^{1-n}\right)}, \tag{19}$$

$$z_5^{'} = \frac{\Pr\left(-z_1z_5 - A\frac{\eta}{2}z_5 - N_bz_5z_7 - N_t(z_5)^2 - Q_0z_4\right)}{\left(1 + \frac{4}{3}Rd\right)}, \tag{20}$$

$$z_7^{'} = -Scz_1z_7 - \frac{N_t}{N_b}z_7^{'} - ScA\frac{\eta}{2}z_7 + \sigma(1 + \delta z_4)^{n^*}z_6\exp\left(-\frac{E_1}{1 + \delta z_4}\right), \tag{21}$$

$$z_9^{'} = -Lbz_1z_9 + Pe[z_9z_7 + (z_8 + \Omega)] - LbA\frac{\eta}{2}z_9, \tag{22}$$

with boundary conditions:

M	Turkyilmazoglu[27]	Present results
0	− 1.000000	− 1.000000
0.5	− 1.224744	− 1.224751
1	− 1.414213	− 1.414216
2.0	− 1.732050	− 1.732060

Table 1. Solution comparison for $f''(0)$ with Turkyilmazoglu[27] when $We = n = \lambda = A = 0$.

No. of grid points in η direction with $\eta = 20$	$f''(0)$	$-\theta'(0)$	$-\phi'(0)$	$-\chi'(0)$
100	0.6853	0.4412	0.7045	0.8066
200	0.6855	0.4415	0.7048	0.8068
400	0.6855	0.4415	0.7048	0.8068
800	0.6855	0.4415	0.7048	0.8068

Table 2. Grid independent test for $We = 0.2, \lambda = 0.1, N_r = 0.4, R_b = 0.2, Pe = 0.1, M = 0.2, N_t = 0.5, N_b = 0.4, Q_0 = 0.2, A = 0.1, n = 0.4, Sc = 0.2$ and $Lb = 0.1$.

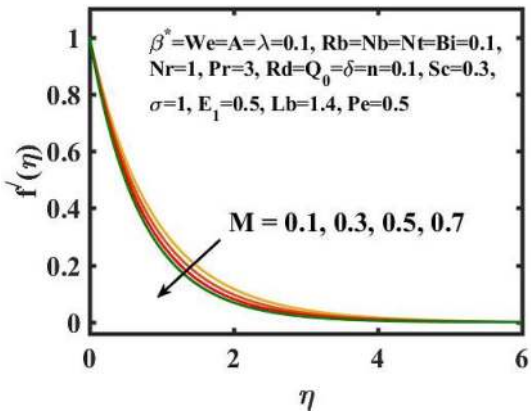

Figure 2. Encouragement of M on $f'(\eta)$.

$$z_1(0) = 0,\ z_2(0) = 1,\ z_5(0) = -Bi[1 + z_4(0)],\ N_b z_7(0) + N_t z_5(0) = 0, z_8(0) = 1, \tag{23}$$

$$z_2(\infty) \to 0,\ z_4(\infty) \to 0,\ z_6(\infty) \to 0,\ z_8(\infty) \to 0. \tag{24}$$

Validation of results

The validation of obtained numerical results via shooting technique has been verified in Table 1 by making comparison with analysis of Turkyilmazoglu[27]. A very excellent accuracy of results is observed between both studies. The grid independent is performed in Table 2 by considering different grid points for η. It is noticed that an excellent solution accuracy has been observed when as number of grid points are increased.

Discussion of results

The transient two-dimensional magnetic flow of Cross nanofluid past a stretching sheet with convective boundary condition, thermal radiation, binary chemical reactions and heat source/sink is considered in the present model. The Buongiorno model incorporated into a currently developed framework for nanofluid. This section manifests the salient features and the rheological behaviour of various flow physical non-dimensional parameters associated in the dimensionless equations. Consideration is engrossed here to point out physical influence of these parameters on velocity, concentration, thermal and motile gyrotactic profiles graphically (Figs. 2, 3, 4, 5, 6, 7, 8, 9, 10, 11, 12, 13, 14, 15, 16, 17, 18, 19, 20, 21 and 22) by varying one parameter and other parameters are kept constant.

Figure 2 depicts the flow control of the M on the velocity profile. Here, increase in M slowdowns the velocity and momentum of the fluid. Practically, it has been noticed that the existence of a magnetic field in the stream field region decelerates the fluid motion. These findings suggest that magnetization force provides additional struggle to the stream which declines its velocity. Figure 3 demonstrates the influence of the We on velocity gradient. Here, it is observed that the rise in We turn down the fluid particles motion slowly. Here, upsurge in material

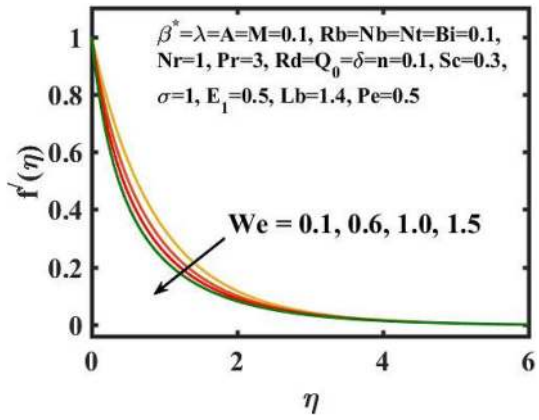

Figure 3. Encouragement of We on $f'(\eta)$.

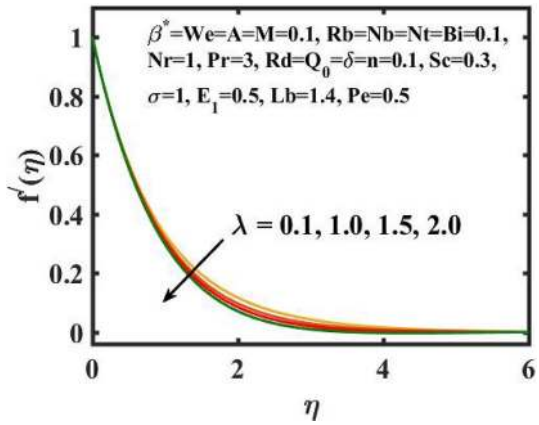

Figure 4. Encouragement of λ on $f'(\eta)$.

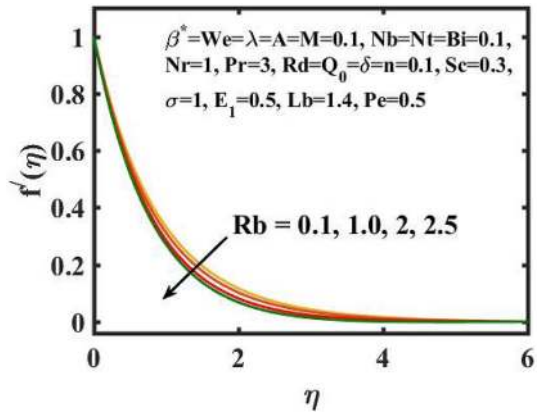

Figure 5. Encouragement of Rb on $f'(\eta)$.

relaxation time affords additional struggle to fluid stream which diminishes the velocity gradient. Figure 4 is devoted to scrutinize the estimation in the velocity profile for several values of λ. Physically, by increasing λ, the inertial force is overcome by the buoyancy force, which results in declination of the velocity gradient. Figure 5 is engrossed to depict the levering of Rb on the velocity gradient. Outcome of the figure reveals that the cumulative values of Rb deteriorates the velocity gradient. This deteriorating behaviour is caused by the fact that Rb is related to the buoyancy force caused by bioconvection, which allows the velocity profile to decay.

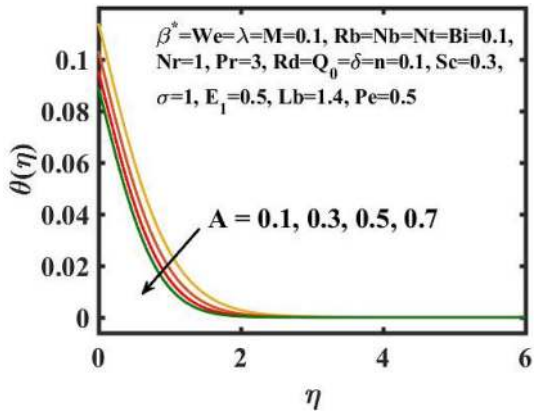

Figure 6. Encouragement of A on $\theta(\eta)$.

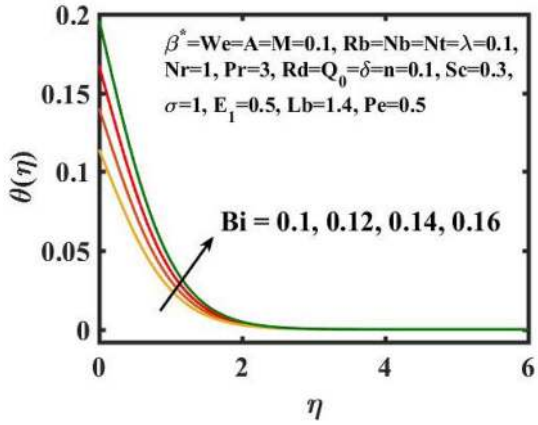

Figure 7. Encouragement of Bi on $\theta(\eta)$.

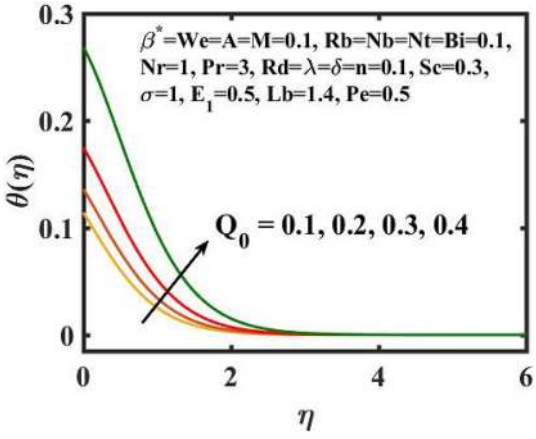

Figure 8. Encouragement of Q_0 on $\theta(\eta)$.

Figure 6 is displayed to envisage the domination of A on the thermal profile. The inclination in A slowdowns the heat transference. Figure 7 manifests the characteristic of Bi on thermal gradient. Here, the increased values of Bi increase the heat transference. Physically describes that even more heating is delivered from the surface to the nanoparticles, resulting in an increase in the temperature gradient. Figure 8 demonstrates the behaviour of Q_0 on temperature profile. The larger Q_0 enhances the thermal profile. In fact, Internal heat generation/absorption either improves or dampens the heat transport. A incremental increase in Q_0 increases thermal gradient,

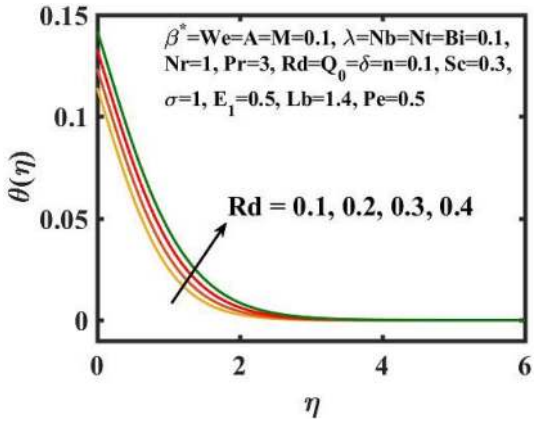

Figure 9. Encouragement of Rd on $\theta(\eta)$.

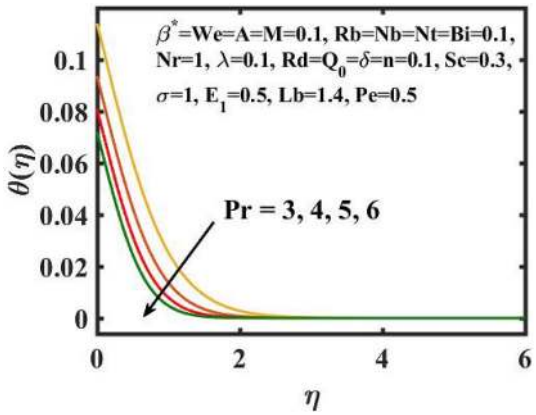

Figure 10. Encouragement of Pr on $\theta(\eta)$.

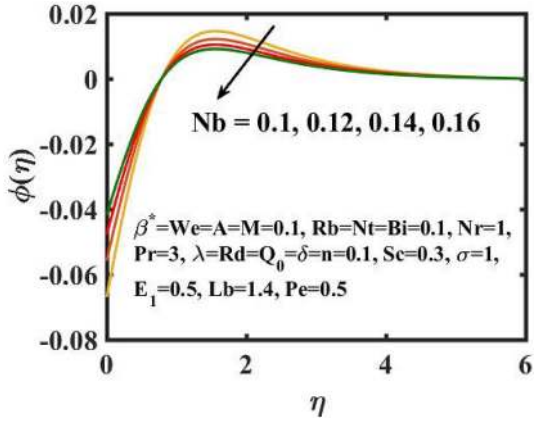

Figure 11. Encouragement of Nb on $\phi(\eta)$.

showing mechanically that an increase in heat source intensity contributes to a greater thermal diffusion layer, which may increase thermal gradient. Figure 9 highlights the outcome of the Rd on thermal profile. The increase in radiation parameter upsurges the thermal distribution. Here, more heat is applied to active liquid due to upshot in radiation phenomenon. As a result, heat transfer escalates.

Figure 10 describes the behaviour of the Pr on thermal profile. The inclination in Pr declines the thermal gradient.Lower Pr equate to higher thermal diffusivity, although higher values result in higher diffusivity. As a

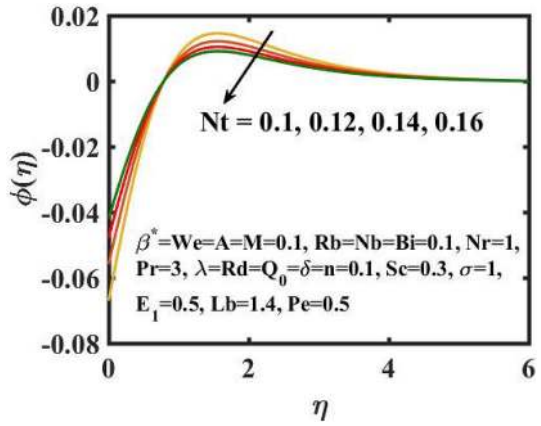

Figure 12. Encouragement of Nt on $\phi(\eta)$.

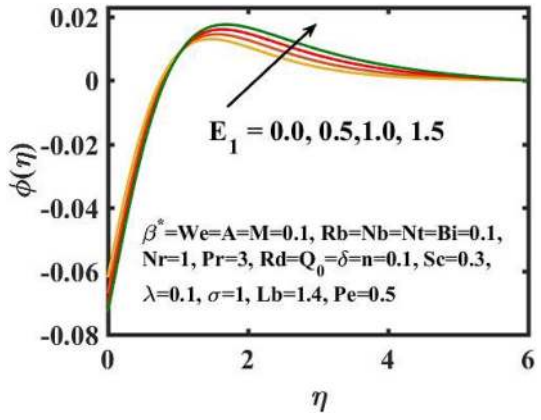

Figure 13. Encouragement of E_1 on $\phi(\eta)$.

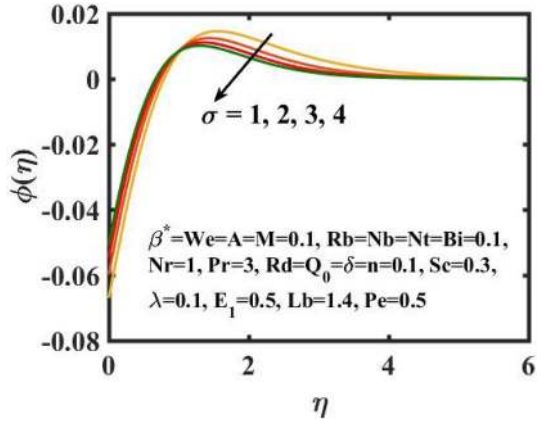

Figure 14. Encouragement of σ on $\phi(\eta)$.

consequence of this justification, the temperature is reduced. Shear thickening activity is characterised by gradual thinning of the boundary layer. Furthermore, by definition, the Pr is inversely related to thermal diffusivity, resulting in a decrease in the thermal profile.

The graphical results for mass transference for varied values of the *Nb* is expressed in Fig. 11. Here, mass distribution diminishes for inclined *Nb*.Concentration gradient decays after more particles are pushed in the reverse way of the solutal distribution to preserve solution homogeneity. Figure 12 determines the sway of *Nt* over concentration gradient. The escalation in *Nt* declines the mass transfer. Physically, raising in the *Nt* causes

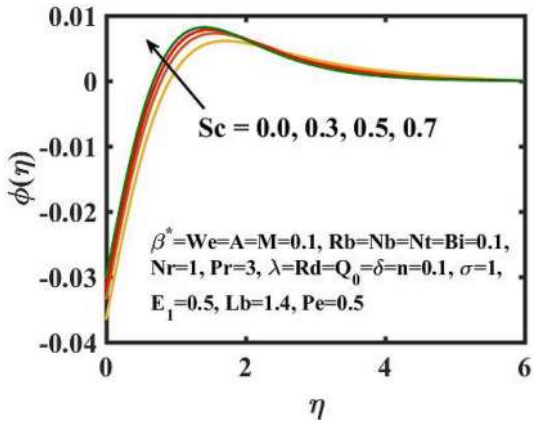

Figure 15. Encouragement of Sc on $\phi(\eta)$.

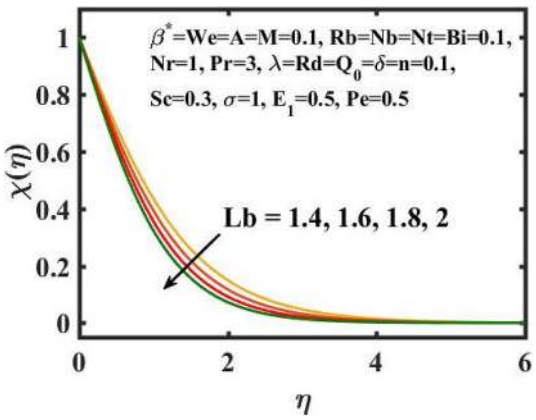

Figure 16. Encouragement of Lb on $\chi(\eta)$.

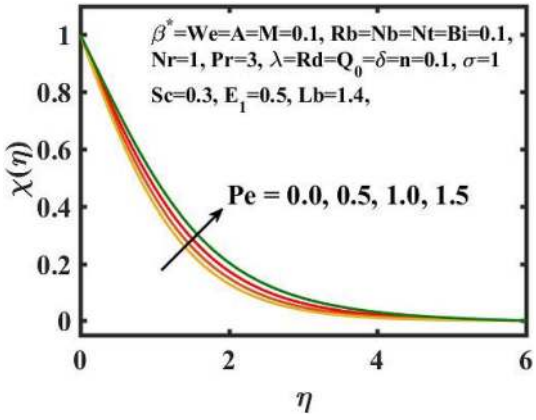

Figure 17. Encouragement of Pe on $\chi(\eta)$.

an increase in thermophoretic energy, which raises the fluid temperature as well as the nanoparticle concentration due to the migration of nanoparticles from warm to chill regions. Figure 13 exhibits the feature of E_1 on concentration distribution. Larger values of E_1 enhances the concentration field. As the E_1 becomes larger, the modified Arrhenius mechanism decays. This eventually inspires the procreative chemical reaction, which causes the concentration of nanoparticles to increase. Figure 14 exemplifies the fluctuation of the concentration field with σ. The concentration of species in the boundary layer decreases as the value of the σ increases. This is because the chemical reaction in this method consumes the chemicals, resulting in a reduction in the

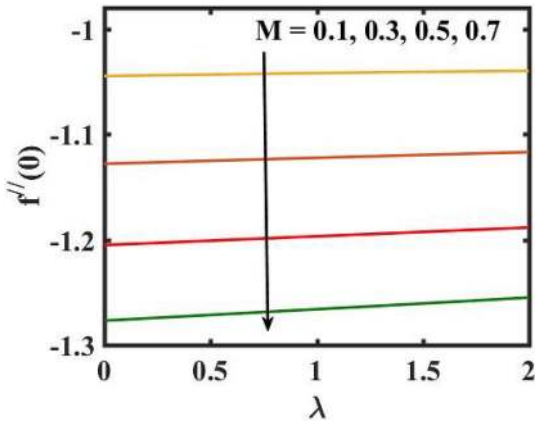

Figure 18. Encouragement of M and λ. on skin friction coefficient.

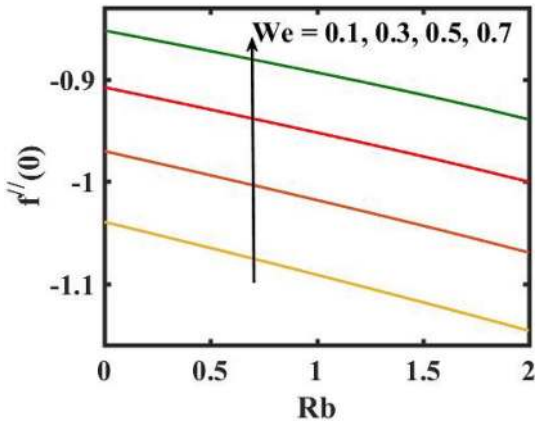

Figure 19. Encouragement We and Rb on skin friction coefficient.

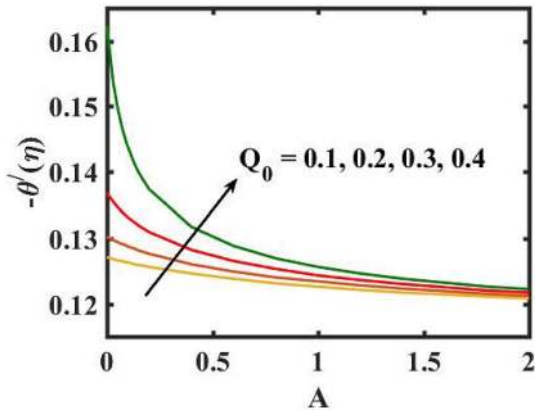

Figure 20. Encouragement of Q_0 and A on local Nusselt number.

concentration profile. Variation in mass transference with respect to Sc is portrayed in Fig. 15. Mathematically, a dimensionless number relating mass diffusivity with momentum diffusivity yielding a fluid flow is treated as Schmidt number. These two terms are physically called as the hydrodynamic thickness layer and mass transport layer. The maximum concentration of nanoparticles corresponds to the smallest Sc.

Figure 16 elucidates the depreciation in the motile microorganism distribution for various values of the Lb. With enlarging value of Lb, a perceptive motile microorganism profile is observed. Figure 17 demonstrates

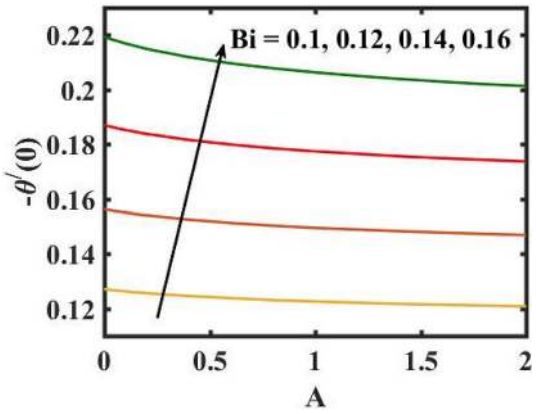

Figure 21. Encouragement of *Bi* and *A* local Nusselt number.

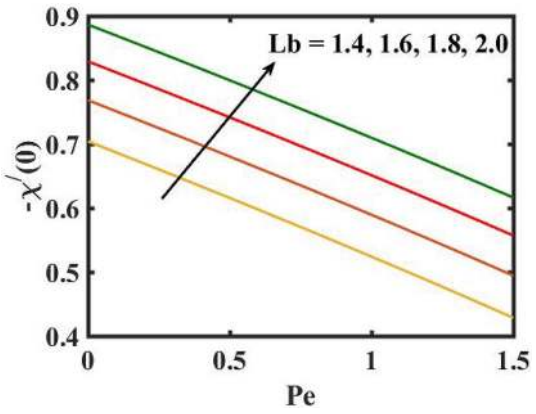

Figure 22. Encouragement of *Lb* and *Pe* on local density number of motile microorganisms.

the impact of the *Pe* on microorganism profile. A rise in *Pe* results in a poorer motile microorganism profile. Increased Pe induces a reduction in the diffusivity of microorganisms and hence a decrease in the motile density of fluid. Figure 18 displays the variation of skin friction coefficient against *M* and λ. Here, escalating values of *M* declines the coefficient of skin friction. Figure 19 shows the skin friction coefficient variation against *We* and *Rb*. Here, escalating values of *We* improves the coefficient of skin friction. The variation of local Nusselt number against Q_0 and *A* is demonstrated in Fig. 20. Here, local Nusselt number upsurges for growing values of Q_0 and declines for escalating values of *A*. The change in local Nusselt number against *Bi* and *A* is established in Fig. 21. Here, local Nusselt number acts as a growing function of *Bi* and declining function of *A*. The change in local density number of motile microorganisms against *Lb* and Pe is established in Fig. 22. Here, density number of motile microorganisms increases for growing values of *Lb* and declines for rise in values of *Pe*. Figures 23 and 24 are sketched for stream functions subject to various flow parameters[28].

Conclusions

The transient magnetic flow of Cross nanofluid past a stretching sheet with convective boundary condition, thermal radiation effects, binary chemical reactions and heat source/sink is considered in the present model. The effect of Brownian motion and thermophoresis is incorporated into a currently developed framework for nanofluid. The salient features and the rheological behaviour of various flow physical parameters on velocity, concentration, thermal and motile gyrotactic profile are deliberated graphically. The key conclusions of the current study are:

- The escalation in *M* and *Rb* slowdowns the velocity and momentum of the fluid.
- The rise in *We* turn down the fluid particles motion slowly.
- The increased values of *Bi* and Q_0 intensify the heat transference.
- The increase in radiation parameter upsurges the thermal boundary but, converse trend is seen for escalating Prandtl number.
- The escalation in *Nt* and *Nb* declines the mass transfer.
- An augmentation in the *Pe* and *Lb* deteriorates themicroorganism profile.
- The local Nusselt number acts as a growing function of Q_0 and *Bi* and declining function of *A*.

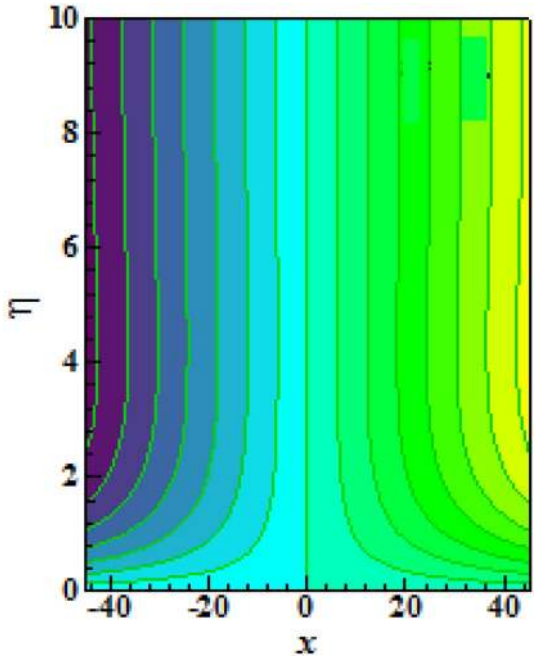

Figure 23. Streamlines for flow parameters when $We = 0.2, \lambda = 0.1, N_r = 0.4, R_b = 0.2, Pe = 0.1, M = 0.2, N_t = 0.5, N_b = 0.4, Q_0 = 0.2, A = 0.1, n = 0.4, Sc = 0.2$ and $Lb = 0.1$.

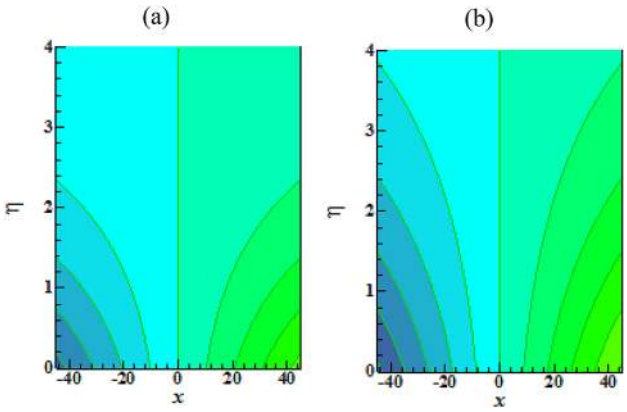

Figure 24. Contour plots of isotherms for when (**a**) $Ha = 0.1$ and (**b**) $Ha = 0.5$.

- The density number of motile microorganisms acts as a growing function of *Lb* and declining function of *Pe*.

Data availability

The data that support the findings of this study are available within the article, the data are made by the authors themselves and do not involve references of others.

Received: 17 April 2021; Accepted: 19 July 2021
Published online: 06 August 2021

References

1. Khan, M. I., Hayat, T., Khan, M. I. & Alsaedi, A. Activation energy impact in nonlinear radiative stagnation point flow of cross nanofluid. *Int. Commun. Heat Mass Transf.* **91**, 216–224. https://doi.org/10.1016/j.icheatmasstransfer.2017.11.001 (2018).
2. Ali, M. *et al.* Computational analysis of entropy generation for cross-nanofluid flow. *Appl. Nanosci.* **10**(8), 3045–3055. https://doi.org/10.1007/s13204-019-01038-w (2020).
3. Abbas, S. Z. *et al.* Mathematical modeling and analysis of cross nanofluid flow subjected to entropy generation. *Appl. Nanosci.* **10**(8), 3149–3160. https://doi.org/10.1007/s13204-019-01039-9 (2020).
4. Xiong, P.-Y. *et al.* Dynamics of multiple solutions of Darcy–Forchheimer saturated flow of cross nanofluid by a vertical thin needle point. *Eur. Phys. J. Plus* **136**(3), 315. https://doi.org/10.1140/epjp/s13360-021-01294-2 (2021).

5. Hamid, A. *et al.* Critical values in axisymmetric flow of magneto-cross nanomaterial towards a radially shrinking disk. *Int. J. Mod. Phys. B* **35**(07), 2150105. https://doi.org/10.1142/S0217979221501058 (2021).
6. Hayat, T., Qasim, M. & Mesloub, S. MHD flow and heat transfer over permeable stretching sheet with slip conditions. *Int. J. Numer. Methods Fluids* **66**(8), 963–975. https://doi.org/10.1002/fld.2294 (2011).
7. Senapati, M., Swain, K. & Parida, S. Numerical analysis of three-dimensional MHD flow of Casson nanofluid past an exponentially stretching sheet. *Karbala Int. J. Mod. Sci.* https://doi.org/10.33640/2405-609X.1462 (2020).
8. Patil, V. S., Patil, A. B., Ganesh, S., Humane, P. P. & Patil, N. S. Unsteady MHD flow of a nano Powell–Eyring fluid near stagnation point past a convectively heated stretching sheet in the existence of chemical reaction with thermal radiation. *Mater. Today Proc.* https://doi.org/10.1016/j.matpr.2020.11.860 (2021).
9. Uddin, I., Ullah, I., Ali, R., Khan, I. & Nisar, K. S. Numerical analysis of nonlinear mixed convective MHD chemically reacting flow of Prandtl–Eyring nanofluids in the presence of activation energy and Joule heating. *J. Therm. Anal. Calorim.* https://doi.org/10.1007/s10973-020-09574-2 (2020).
10. Nayak, M. K. *et al.* Entropy optimized MHD 3D nanomaterial of non-Newtonian fluid: A combined approach to good absorber of solar energy and intensification of heat transport. *Comput. Methods Programs Biomed.* **186**, 105131. https://doi.org/10.1016/j.cmpb.2019.105131 (2020).
11. Khan, M., Irfan, M., Khan, W. A. & Alshomrani, A. S. A new modeling for 3D Carreau fluid flow considering nonlinear thermal radiation. *Results Phys.* **7**, 2692–2704. https://doi.org/10.1016/j.rinp.2017.07.024 (2017).
12. Hashim, A., Hamid, M. K. & Khan, U. Thermal radiation effects on Williamson fluid flow due to an expanding/contracting cylinder with nanomaterials: Dual solutions. *Phys. Lett. A* **382**(30), 1982–1991. https://doi.org/10.1016/j.physleta.2018.04.057 (2018).
13. Ali, U., Malik, M. Y., Alderremy, A. A., Aly, S. & Rehman, K. U. A generalized findings on thermal radiation and heat generation/absorption in nanofluid flow regime. *Phys. Stat. Mech. Appl.* **553**, 124026. https://doi.org/10.1016/j.physa.2019.124026 (2020).
14. Gnaneswara Reddy, M., Punith Gowda, R., Naveen Kumar, R., Prasannakumara, B. & Ganesh Kumar, K. Analysis of modified Fourier law and melting heat transfer in a flow involving carbon nanotubes. *Proc. Inst. Mech. Eng. Part E J. Process Mech. Eng.* https://doi.org/10.1177/09544089211001353 (2021).
15. Xiong, P.-Y. *et al.* Comparative analysis of (Zinc ferrite, Nickel Zinc ferrite) hybrid nanofluids slip flow with entropy generation. *Mod. Phys. Lett. B* https://doi.org/10.1142/S0217984921503425 (2021).
16. Merkin, J. H. Natural-convection boundary-layer flow on a vertical surface with Newtonian heating. *Int. J. Heat Fluid Flow* **15**(5), 392–398. https://doi.org/10.1016/0142-727X(94)90053-1 (1994).
17. Rasool, G. *et al.* Entropy generation and consequences of binary chemical reaction on MHD Darcy–Forchheimer Williamson nanofluid flow over non-linearly stretching surface. *Entropy* **22**(1), 1. https://doi.org/10.3390/e22010018 (2020).
18. Wang, J. *et al.* Entropy optimized stretching flow based on non-Newtonian radiative nanoliquid under binary chemical reaction. *Comput. Methods Programs Biomed.* **188**, 105274. https://doi.org/10.1016/j.cmpb.2019.105274 (2020).
19. Punith Gowda, R. J. *et al.* Computational modelling of nanofluid flow over a curved stretching sheet using Koo–Kleinstreuer and Li (KKL) correlation and modified Fourier heat flux model. *Chaos Solitons Fractals* **145**, 110774. https://doi.org/10.1016/j.chaos.2021.110774 (2021).
20. Ijaz Khan, M. & Alzahrani, F. Activation energy and binary chemical reaction effect in nonlinear thermal radiative stagnation point flow of Walter-B nanofluid: Numerical computations. *Int. J. Mod. Phys. B* **34**(13), 2050132. https://doi.org/10.1142/S0217979220501325 (2020).
21. Khan, M., Salahuddin, T., Malik, M. Y., Alqarni, M. S. & Alqahtani, A. M. Numerical modeling and analysis of bioconvection on MHD flow due to an upper paraboloid surface of revolution. *Phys. Stat. Mech. Appl.* **553**, 124231. https://doi.org/10.1016/j.physa.2020.124231 (2020).
22. Chu, Y.-M. *et al.* Significance of activation energy, bio-convection and magnetohydrodynamic in flow of third grade fluid (non-Newtonian) towards stretched surface: A Buongiorno model analysis. *Int. Commun. Heat Mass Transf.* **118**, 104893. https://doi.org/10.1016/j.icheatmasstransfer.2020.104893 (2020).
23. Al-Khaled, K., Khan, S. U. & Khan, I. Chemically reactive bioconvection flow of tangent hyperbolic nanoliquid with gyrotactic microorganisms and nonlinear thermal radiation. *Heliyon* **6**(1), e03117. https://doi.org/10.1016/j.heliyon.2019.e03117 (2020).
24. Hashem Zadeh, S. M., Mehryan, S. A. M., Sheremet, M. A., Izadi, M. & Ghodrat, M. Numerical study of mixed bio-convection associated with a micropolar fluid. *Therm. Sci. Eng. Prog.* **18**, 100539. https://doi.org/10.1016/j.tsep.2020.100539 (2020).
25. Waqas, H., Khan, S. U., Shehzad, S. A., Imran, M. & Tlili, I. Activation energy and bioconvection aspects in generalized second-grade nanofluid over a Riga plate: A theoretical model. *Appl. Nanosci.* **10**(12), 4445–4458. https://doi.org/10.1007/s13204-020-01332-y (2020).
26. Khan, M. I., Kadry, S., Chu, Y. M., Khan, W. A. & Kumar, A. Exploration of Lorentz force on a paraboloid stretched surface in flow of Ree-Eyring nanomaterial. *J. Mater. Resear. Technol.* **9**, 10265–10275 (2020).
27. Turkyilmazoglu, M. The analytical solution of mixed convection heat transfer and fluid flow of a MHD viscoelastic fluid over a permeable stretching surface. *Int. J. Mech. Sci.* **77**, 263–268 (2013).
28. Mabood, F., Khan, S. U. & Tlili, I. Numerical simulations for swimming of gyrotactic microorganisms with Williamson nanofluid featuring Wu's slip, activation energy and variable thermal conductivity. *Appl. Nanosci.* https://doi.org/10.1007/s13204-020-01548-y (2020).

Acknowledgements

This research was supported by Basic Science Research Program through the National Research Foundation of Korea (NRF) funded by the Ministry of Education (No. 2017R1D1A1B05030422).

Author contributions

The research work of the subject paper was performed under the supervision of Principle investigator Dr. M.I.K. and Co-investigator A.H. The authors S.U.K. and R.N.K. have done formal analysis and software package respectively. The authors R.J.P.G. and B.C.P. have writing the original draft. The authors Q.-H.S., N.A.S. and J.D.C. have review and edit the final version. Further, the results are improved and compared with previous literatures as suggested by reviewers are done through these authors.

Competing interests

The authors declare no competing interests.

Additional information

Correspondence and requests for materials should be addressed to N.A.S.

Reprints and permissions information is available at www.nature.com/reprints.